19th Brazilian Congress of Thermal Sciences and Engineering
November 06th-10th, 2022, Bento Gonçalves - RS - Brazil

ENC-2022-0655
COMPUTATIONAL FLUID DYNAMICS ANALYSES TO IMPROVE PORTABLE DUCED FAN PERFORMANCE FOR CROPS SPRAY PROTECTION

Guillermo Campello Fernandez O'Keeffe
Vicente Luiz Scalon
São Paulo State University – Bauru Campus
guillermo.campello@unesp.br; scalon@feb.unesp.br

Rodolfo Castanho Fernandes
Institute of Eletrical and Eletronics Engineers
rodolfocf@ieee.org

Abstract. *For pest and disease control in agriculture, products (chemical or organically) are used for plant protection. Depending on the classification of the sprayed product in the crop, several droplets must reach the surface area of the leaf, to guarantee its protection (herbicides must reach 20 to 30 droplets for each centimeter square). As there are several types of leaf structures, the spray droplet may not penetrate satisfactorily in all types of crops, due to the high leaf density in some of them, and it may leave part of the crop unprotected. To increase the spray droplet penetration into denser crops, ventilation is used in spraying. In this way, the air flow causes a certain excitation in the leaves, allowing the sprayed product to reach leaves in the center of the crop. In the past, the interior of denser regions could be reached with greater applications of products, which resulted in a high consumption of product per hectare. With the advent of Precision Agriculture, studies to reduce agricultural defensive consumption per hectare were increasingly carried out, and new application technologies were emerging. Among them, the aid of air in spraying. For crops where management is possible with tractor-operated sprayers, many solutions have already been developed. To serve the small producer, who does not need to have tractor-operated sprayer, as well as to enable spraying in regions where such equipment cannot arrive, it is necessary a portable sprayer that is assisted by air. For this, a fan is necessary to produce the air flow excitation in the crop. To meet the ergonomic requirement of a portable sprayer, where the target is the smallest size of ducted fan possible, and the productivity requirement for agriculture, CFD will enhance the design exploration of a proposed ducted fan (rotational speed higher than 15,000 rpm), where the velocity of the air flow in the crop must be effective to leaf excitation, with the lowest power consumption, to increase the efficiency of the fan.*

Keywords: *Computational fluid dynamic (CFD), Turbomachinery, Efficiency, Agricultura machinery*

1. INTRODUCTION

Computational fluid dynamics (CFD), numerical analysis and simulation tools of fluid flow processes have emerged from the development stage and become nowadays a robust design tool. It is widely used to study various transport phenomena which involve fluid flow, heat, and mass transfer, providing detailed information for spatial and temporal distributions of flow speed and direction, pressure, temperature and species concentration. The CFD tools provide a cost-effective way of carrying out equipment and process design and optimization and can reduce risk in equipment modification and process scale-up. In recent years, CFD modeling has been gaining attraction from the agri-food industry (Bartzanas et al, 2013).

In this way, the CAE technology (which includes computational fluid dynamics (CFD), finite element analysis (FEA) and discrete element analysis (DEM)) is carrying out to provide answers before any practical experiment is made. The consequence is a short, cheaper, and reliable methodology to development products (stresses and lifetime), study processes (chemicals, heat transfer and fluid flow) and also optimize resources.

Chemical pesticides provide an effective approach to ensure crop yields. However, their excessive use and off-target drift can cause concerns over food safety and environmental pollution. Improving the safety and reducing the environmental impacts of pesticide use is crucial for sustainable agricultural development. Part of reducing environmental

impact is the proper selection of settings for spray parameters can effectively reduce off-target deposition and improve efficacy (Zhang et al, 2022; Foqué et al, 2012).

According to this, the assisted air flow leads a large impact on the results of the spray treatment with respect to penetration of the product into the vegetation or treatment on the underside of the leaves (Pérez-Ruiz et al, 2011).

Using a turbomachinery device for assisting the spray deposition, it is possible to reach areas of vegetation that without the assistance was not possible. For this reason, this type of machinery is used in high density morphology vegetations. For portable sprayer, this kind of device is not common, since it is possible to spray inside the vegetation by positioning the nozzle inside it, which will increase the time for spraying, and then reducing the operational efficiency of the spray operation. Other solution is spray with high pressure nozzles, which will increase the consumption of product.

The use of the CAE technology provides a wide range of solutions to be tested. The ultimate aim of developments in the CFD field is to provide a capability comparable with other CAE (computer-aided engineering) tools such as stress analysis codes. The main reason why CFD has lagged behind is the tremendous complexity of the underlying behavior, which precludes a description of fluid flows that is at the same time economical and sufficiently complete. The availability of affordable high-performance computing hardware and the introduction of user-friendly interfaces have led to a recent upsurge of interest, and CFD has entered into the wider industrial community since the 1990s (Versteeg and Malalasekera, 1995). The following are the equations which governs the time-dependent three-dimensional fluid flow and heat transfer of compressible Newtonian fluid.

Mass Conservation

$$\frac{\partial \rho}{\partial t} + div(\rho u) = 0 \qquad (1)$$

ρ – density
u -velocity

Momentum Equation in X

$$\frac{\partial (\rho u)}{\partial t} + div(\rho u u) = -\frac{\partial P}{\partial x} + div(\mu grad u) + S_{Mx} \qquad (2)$$

S – net source X
P - pressure

Momentum Equation in Y

$$\frac{\partial (\rho v)}{\partial t} + div(\rho v u) = -\frac{\partial P}{\partial y} + div(\mu grad v) + S_{My} \qquad (3)$$

S – net source Y

Momentum Equation in Z

$$\frac{\partial (\rho w)}{\partial t} + div(\rho w u) = -\frac{\partial P}{\partial z} + div(\mu grad w) + S_{Mz} \qquad (4)$$

S – net source Z

Energy Equation

$$\frac{\partial (\rho i)}{\partial t} + div(\rho i u) = -P div u + div(k grad T) + \phi + S_i \qquad (5)$$

P – pressure
k – thermal conductivity
T – temperature
Φ – viscous dissipation

2. EXPERIMENTAL TEST PROCEDURE

The experimental procedure was performed by a portable sprayer with assisted air. The assisted air device is composed by an axial ducted fan. The sprayer's model below (Fig.1) is used for chemicals applications, and with the air assistance it reaches up to 4.5 meters. For this purpose, the experiment is going to measure the air velocity in the outlet of the nozzle.

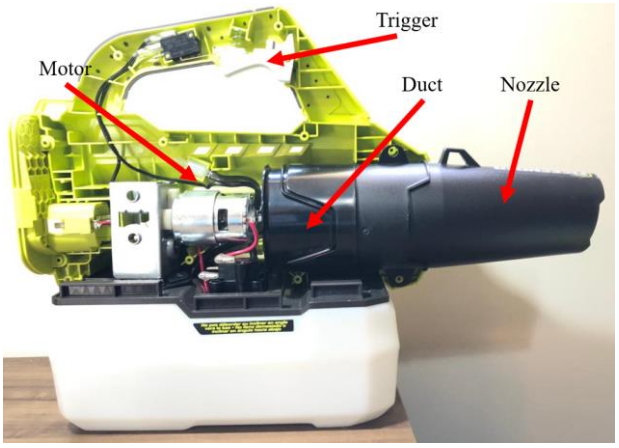

Figure 1. Sprayer air assisted components

Although the sprayer is battery powered, it was connected to a DC power supply to ensure and measure the power input. The electric motor was powered by a Minipa MPL-3305M DC power supply. The rotational speed of the motor shaft was measured by a Minipa MDT-2238A digital photo/contact tachometer. Figure 2 shows the position of the reflective sticker to measure the rotational speed (ω_r). The air flow speed (V_n) was measured by Testo 405i thermal anemometer. It was used to measure the airflow speed in the center of the nozzle exit, and the in several distances ahead. The distance between the measurement points is 100 mm (where *n* indicates the distance to the nozzle exit).

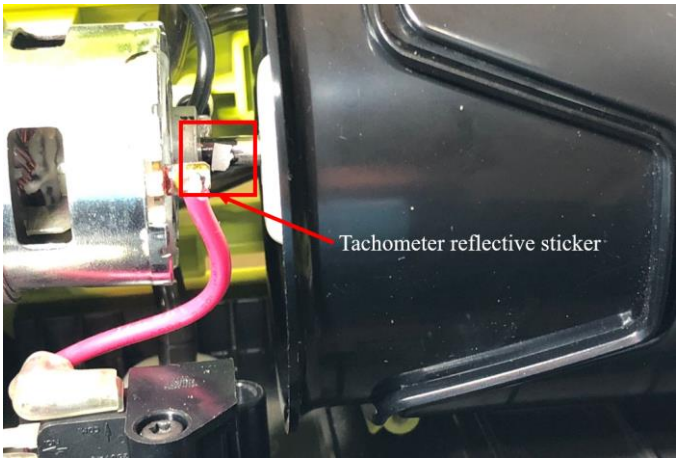

Figure 2. Tachometer reflective sticker mounting position

2.1 Experimental test results

After performing the tests discussed in chapter 2, the results are the following:

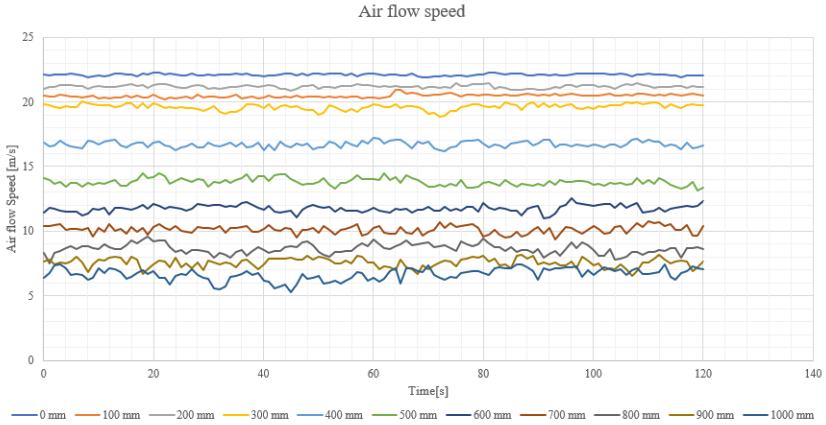

Figure 3. Air flow speed for each distance measured from the nozzle

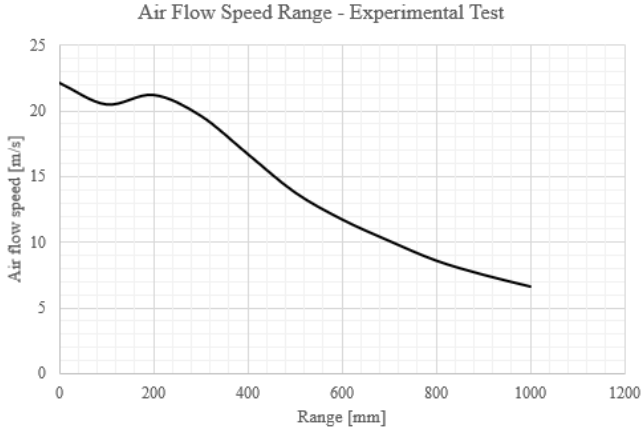

Figure 4. Air flow speed by the distance range in experimental test

The measured rotation speed in the digital tachometer is 16,500 rpm (for the MRF file application, must be considered 1730 rad/s).

3. NUMERICAL TEST PROCEDURE

After the experimental procedure is done, the sprayer was opened, and the main components of the assisted air system were measured by caliper. The most complex component of the system is the axial fan. For this reason, a meshing points was proposed in the fan surface, to be scanned and generates a CAD file.

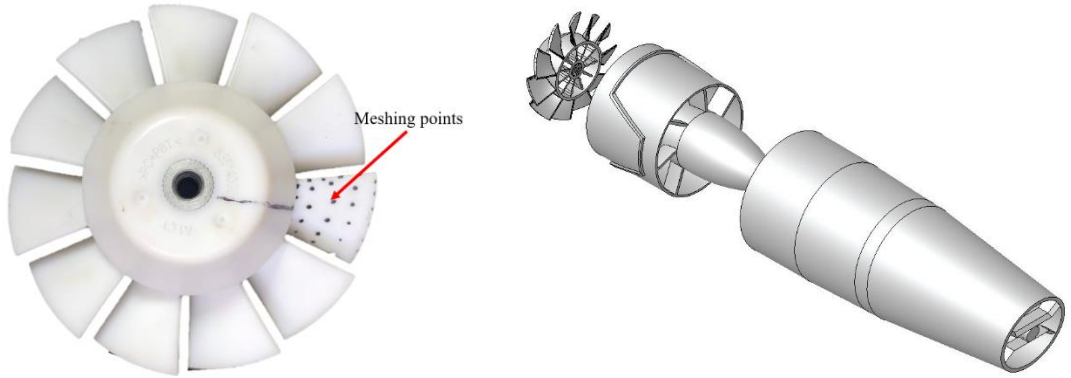

Figure 5. Fan meshing points (left). CAD assembly file (right)

After measuring all the components, a CAD assembly file is created. This assembly is composed by fan, duct, and nozzle geometries. To apply the generated geometries for a CFD analysis, a STL (stereolithography) file must be created. For a better CFD meshing generation, instead of generating one assembly file with all components inside, a STL file of each component gives more accurate mesh size for cells with small edges.

For creating a CFD analysis using OpenFOAM®, the setup of the simulation must be divided in 3 (three) parts: 0 (zero), constant and system. In the 0 folder, the boundary conditions (pressure and velocity) and turbulence terms (*k*, *nut* and *omega* for the turbulence model κ-ω) are applied to each patch of the model. In the constant folder, the geometry (STL's file), the turbulence model, transport properties of the fluid (in case of the air, it is the kinematic viscosity) and the MRF (multiple Reference Frame) file. And for the system folder, it is where all the set up and control of the simulation are storage.

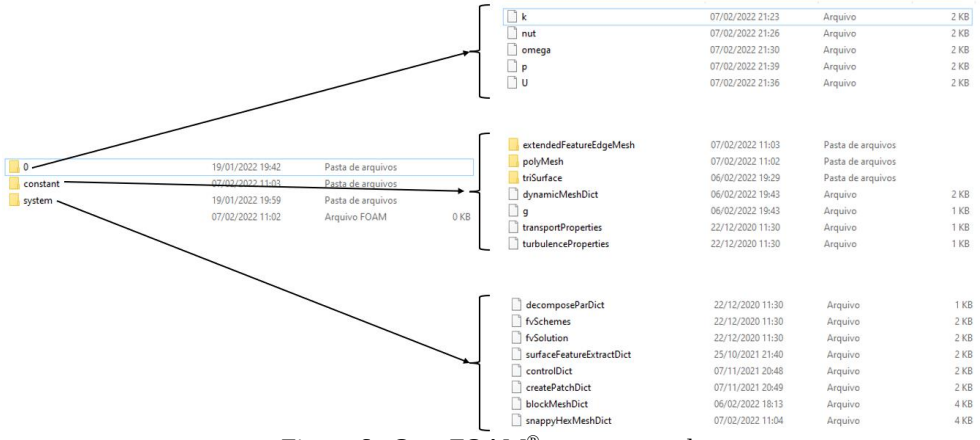

Figure 6. OpenFOAM® set up example

Considering that we already have a start point of velocity to check the turbulence terms, we can calculate the terms of the 0 folder like below:

$$\nu_t = 0{,}09\frac{(k)^2}{\varepsilon} \tag{6}$$

$$\varepsilon = 0{,}09\frac{3}{4}\frac{(k)^{3/2}}{l} \tag{7}$$

$$k = \frac{3}{2} * \left(U_{ref} * T_i\right)^2 \tag{8}$$

The MRF file is responsible for the multiple reference frame. In this method, the whole region is sub-divided into one or more rotating zones and one stationary zone. This approach considers the rotation of wall (impeller) without moving the mesh by making necessary changes in the momentum equation. The velocity field with respect to inertial frame (stationary zone) is u and the relative velocity in the rotating zone is u_r. The absolute velocity and relative velocity in each zone are related as:

$$\overrightarrow{u_r} = \vec{u} - (\vec{\Omega} \times \vec{r}) \tag{9}$$

where Ω is the rotation speed and r is the vector pointing from rotation center to the point of evaluation of relative velocity. The momentum equation is solved for absolute velocity with convective fluxes that accounts for the rotation of the rotating zones (by making fluxed relative to stationary frame in all zones). The left-hand side of momentum equation (for a single-phase flow) becomes:

$$\frac{\partial}{\partial x}(\rho\vec{u}) + \nabla.(\rho\vec{u}_r\vec{u}) + \rho(\vec{\Omega} \times \vec{u}) = RHS \tag{10}$$

where ρ ($\Omega^{\rightarrow} \times u^{\rightarrow}$) is the Coriolis force. The face fluxed are made relative by the following equation:

$$phi_r = phi - \rho(\vec{\Omega} \times \vec{r})S \tag{11}$$

where the relative flux of cells and relative velocity of the cells located in the stationary zone ($\Omega^{\rightarrow}$=0) are reduce to absolute flux and velocity (OpenFOAM® user guide).

After assigning the rotation in the MRF file (the unit is rad/s), it is possible to generate the mesh after the commands blockMesh (responsible to generate the hexahedral volume mesh, and where the patches and boundary conditions are created), surfaceFeatureExtract (responsible for capture the STL file and import them to the CFD model), and for last, snappyHexMesh (responsible to interpolate the surfaces imported to model, and generate the mesh with the with the correspondent necessary mesh size, refinement regions, by the castellation and snapping process. Following is the mesh generated for this analysis.

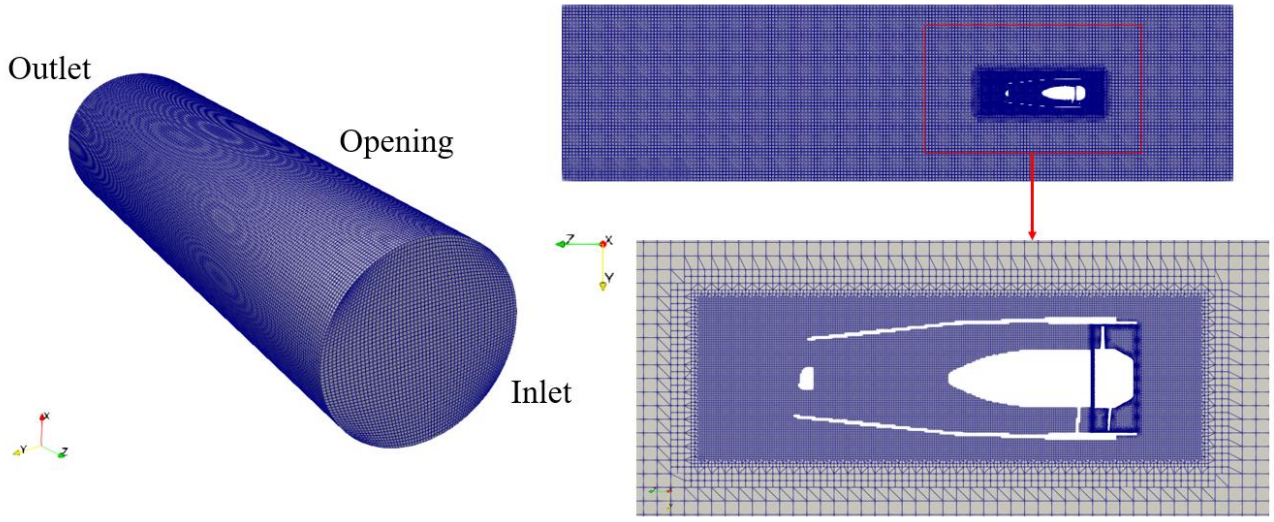

Figure 7. Proposed mesh

The overall volume is consisted by a cylinder with the inlet of the fan and borders (opening) with 3 (three) times the fan diameter. The cylinder outlet is located 1.1 meters ahead of the nozzle exit.

The turbulence model considered for this simulation was the k-ω SST model. The mesh validation is made by the function checkMesh, and it checks the mesh parameters assigned in the snappyHexMesh file.

After the mesh, and check the mesh parameters, the analysis is ready to run. The calculation can be performed in multiple cores if the hardware is capable. For this analysis was used the simpleFOAM solver, capable to calculate turbulent steady-state analysis. In order to ensure that the simulation will not crash, a small time step was considered. In this case, the time step is 0.001 second. The results were storage in the memory after each 1,000 steps (each 1 (one) second has its results). Also, for a better residual in continuity, a table was considered in the MRF file to speed up the rotation of the fan, while the total time increases. The table is in following figure:

```
MRFchec
{
    cellZone    cellMRFzone;
    active      yes;

    // Fixed patches (by default they 'move' with the MRF zone)
    nonRotatingPatches ();

    origin    (0.0 0.0 0.0);
    axis      (1 0 0);
    omega     table //constant -1730;
    (
        (0 0)
        (0.01 -0.01)
        (0.02 -0.05)
        (0.04 -1)
        (2.5 -2)
        (5 -5)
        (10 -50)
        (15 -200)
        (20 -600)
        (25 -1730)
    );
}
```

Figure 8 - MRF table for increasing the rotational speed [rad/s]

3.1 Numerical test result

After performing the numerical test discussed in chapter 3, the results are the following:

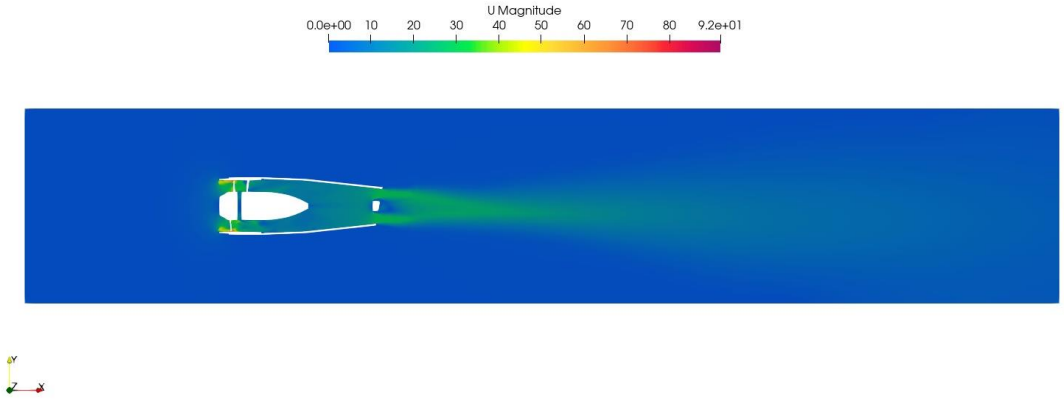

Figure 9. *U* magnitude in the XY central plane

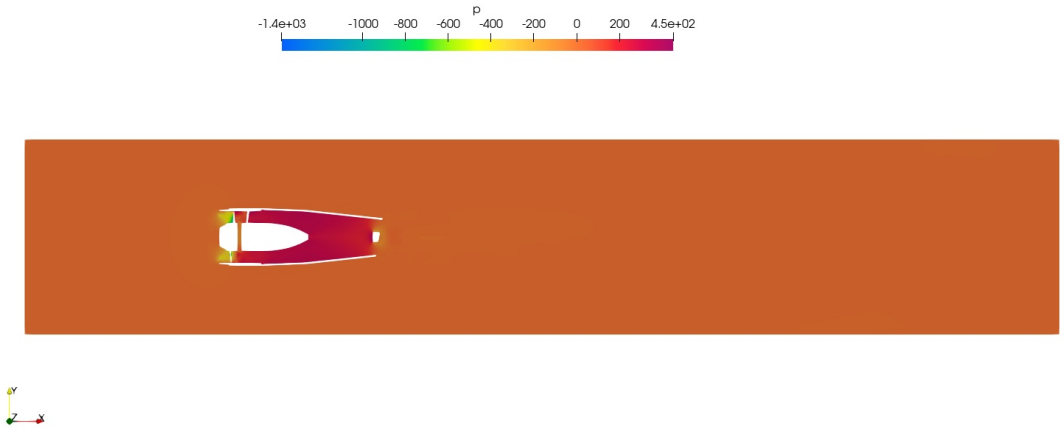

Figure 10. Pressure in XY central plane

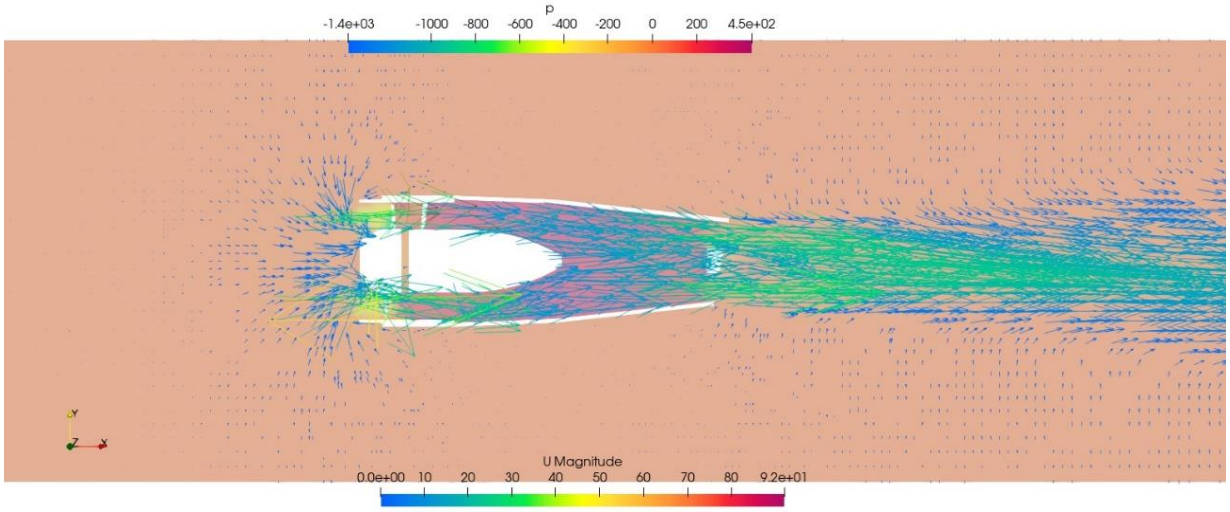

Figure 11. Pressure contour and U magnitude vectors

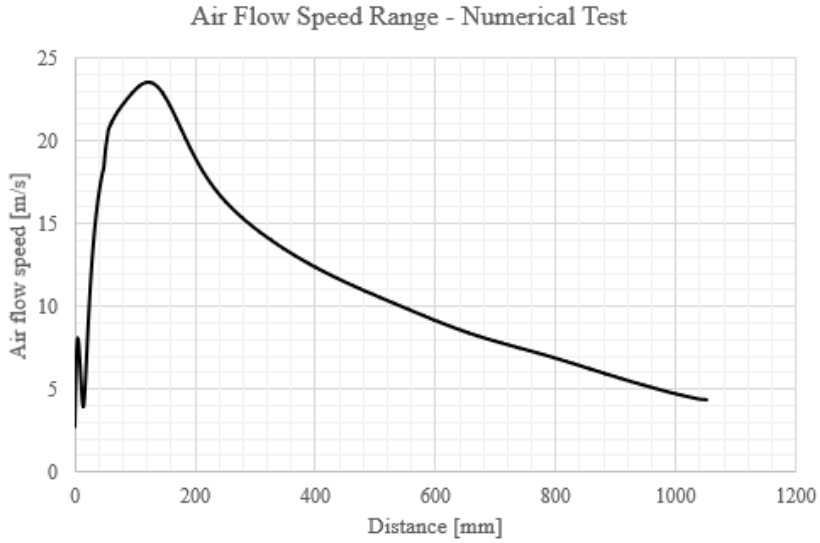

Figure 12. Air flow speed by the distance range in numerical test

By the results shown in the figures above is possible to observe the correct orientation of rotation of the fan, generating a low-pressure region in the inlet of the fan. This region creates the suction area of the fan, and then it provides velocity to air by the pressure increase (Figure 10 plots the pressure rise of the fan). In figure 11 it is possible to see a region of air recirculation created by wall design in the inlet of the duct. By changing duct inlet design, and arranging a smooth round fillet, it may decrease the recirculation of air and decrease the pressure loss in the inlet region of the fan.

Figure 9 show the velocity plot in the XY plane. It is possible to see the influence of the narrow outlet diameter in the air flow spread in the Y axis. The flow in the X axis is shown in Figure 12. The curve change close to 0 mm is due to the nozzle in the center of the outlet. It interrupts the air flow in the X axis, and creates a recirculation area forward it.

4. RESULTS AND DISCUSSION

After running the first simulation, a second trial was set, but with the time step changed to 0.005 secondsm instead of the 0.001 second of the first trial. The solver was able to calculate the simulation without crash by high resisual levels. The total time of the calculation decreased from 168 hours total time to 36 hours (21% of the total time of the first trial).

Considering the results in the chapter 2.1 and 3.1, we can summarize them in the following table:

Table 1. Comparison between experimental and numerical test

	Distance ahead nozzle exit [m]				
	0,2	0,4	0,6	0,8	1,0
Speed @ Experimental Result [m/s]	21,18	16,71	11,75	8,62	6,66
Speed @ Numerical Result [m/s]	19,00	12,36	9,13	6,85	4,69
Difference Experimental / Numerical [m/s]	2,18	4,35	2,62	1,77	1,97
Error	10,27%	26,01%	22,28%	20,54%	29,52%

By the results in table 1 it is possible to plot the following chart:

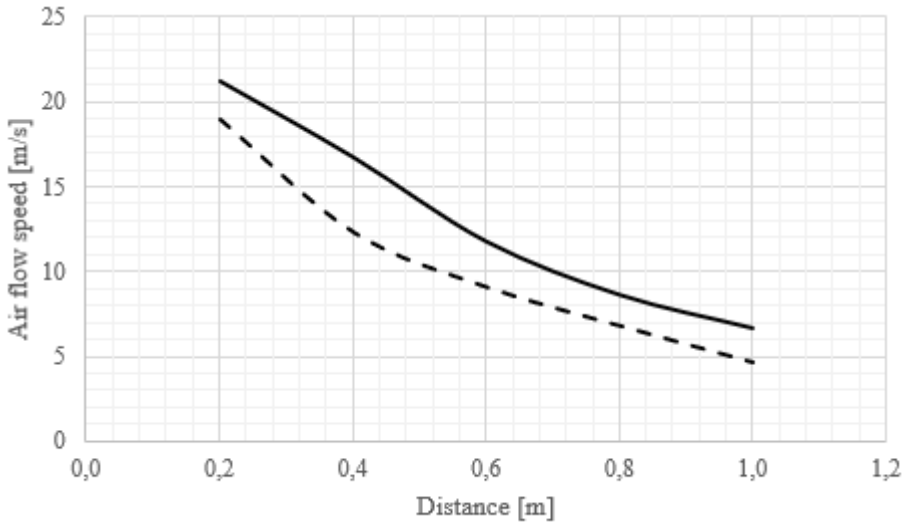

Figure 13. Experimental result versus numerical result

5. CONCLUSIONS

It is possible by analyzing results that the difference between the experimental test and numerical test is 2.6 m/s (average). Considering this difference (between the experimental and numerical test) is possible to arrange new analyses of axial fan geometry and get an estimated result of how it would perform in an experimental test.

In this case was not considered the generation of the boundary layer. This condition must be analyzed in further studies to discover its impacts in the difference of the experimental and numerical test.

For the time step change, it was possible to prove that this analysis case can be run with a time step of 0.005, which will result in a faster calculation until the rotational speed applied in the MRF file.

For further simulations, it will be necessary implement the propellerInfo function object by OpenFOAM®. It will be essential to analyze the power consumption of the fan in the operating proposed condition. And then calculate the fan efficiency.

6. REFERENCES

BARTZANAS, T. et al. Computational fluid dynamics applications to improve crop production systems. *Computers and Electronics in Agriculture*, v. 93, p. 151–167, abr. 2013.

BADULES, J. et al. Comparative study of CFD models of the air flow produced by an air-assisted sprayer adapted to the crop geometry. *Computers and Electronics in Agriculture*, v. 149, p. 166–174, jun. 2018.

ZHANG, C. et al. Wind tunnel study of the changes in drag and morphology of three fruit tree species during air-assisted spraying. *Biosystems Engineering,* v. 218, p. 153–162, jun. 2022.

FOQUÉ, D.; PIETERS, J. G.; NUYTTENS, D. Spray deposition and distribution in a bay laurel crop as affected by nozzle type, air assistance and spray direction when using vertical spray booms**.** *Crop Protection*, v. 41, p. 77–87, nov. 2012.

PÉREZ-RUIZ, M. et al. Optimization of agrochemical application in olive groves based on positioning sensor**.** *Precision Agriculture*, v. 12, n. 4, p. 564–575, 22 out. 2010.

VERSTEEG, H. K.; W MALALASEKERA. *An introduction to computational fluid dynamics: the finite volume method*. Harlow: Pearson Education, 2011.

DATE, A. W. *Introduction to computational fluid dynamics*. New York: Cambridge University Press, 2005.

DE, A. *Técnicas computacionais para dinâmica dos fluídos: conceitos básicos e aplicações.* São Paulo: Edusp, 2000.

OpenFOAM® - Documentation Guide < https://www.openfoam.com/documentation/user-guide>

7. RESPONSIBILITY NOTICE

The authors are the only responsible for the printed material included in this paper.